Journal of Power Sources 244 (2013) 747–751

Contents lists available at SciVerse ScienceDirect

Journal of Power Sources

journal homepage: www.elsevier.com/locate/jpowsour

Short communication

Free-standing heterogeneous hybrid papers based on mesoporous γ-MnO_2 particles and carbon nanotubes for lithium-ion battery anodes

Young Soo Yun [a], Jung Min Kim [b], Hyun Ho Park [a], Jaehoon Lee [a], Yun Suk Huh [b], Hyoung-Joon Jin [a,*]

[a] Department of Polymer Science and Engineering, Inha University, Incheon 402-751, Republic of Korea
[b] Division of Materials Science, Korea Basic Science Institute (KBSI), Daejeon 305-333, Republic of Korea

HIGHLIGHTS

- ► Free-standing anodes for lithium ion battery were successfully prepared.
- ► These anodes are substrate- and binder-free with high flexibility and conductivity.
- ► The mesoporous γ-MnO_2 particles were well-dispersed throughout all the anodes.
- ► A high reversible capacity of 934 mA h g^{-1} (0.01–3.0 V) was maintained after 150 cycles.

ARTICLE INFO

Article history:
Received 15 October 2012
Received in revised form
14 November 2012
Accepted 16 November 2012
Available online 23 November 2012

Keywords:
Hybrid
Anode
Lithium-ion battery
Carbon nanotube
Manganese oxide

ABSTRACT

Free-standing heterogeneous hybrid papers based on mesoporous γ-MnO_2 particles and acid-treated single-walled carbon nanotubes (a-SWCNTs) for lithium-ion battery anodes are successfully prepared by simple vacuum filtration. The mesoporous γ-MnO_2 particles with high surface areas are well dispersed throughout these anodes by being bound in nanoporous a-SWCNT networks. Furthermore, these anodes exhibit a high electrical conductivity of 2.5×10^2 S cm^{-1} with high flexibility, which makes them substrate- and binder-free. For 50 wt% mesoporous γ-MnO_2 particle-loaded anodes, a high reversible capacity of 934 mA h g^{-1} (0.01–3.0 V) is maintained after 150 cycles.

1. Introduction

Nanostructured design of electrode materials is becoming increasingly important for advanced electrochemical energy storage devices because of the unusual physical and electrical properties endowed by confining the dimensions of such materials [1–3]. Among the great number of nanostructured materials, carbon nanotubes (CNTs) have received a great deal of attention due to their excellent electrical, mechanical, and thermal properties [4–9], and many strategies involving the use of CNTs have been proposed to make advanced battery electrodes [10–18]. Free-standing CNT electrodes in particular have strong points; for example, they have no need for binders such as polyvinylidene fluoride or current collectors such as copper (~10 mg cm^{-2}) and aluminum (5 mg cm^{-2}), and they exhibit high flexibility. They also have an advantage in terms of mass transfer and the amount of active area due to their nanoporous morphologies [16–18]. However, the electrode systems composed of only CNTs have low capacity compared to heterogeneous hybrid systems.

Various transition metal oxides have been widely studied as anode materials for lithium-ion batteries (LIB) because of their high capacitance, great capacity retention, and high discharging rates [19–27]. Manganese oxide (MnO_2) in particular has attracted attention as an electrode for LIBs due to its high storage capacity, low cost, environmental friendliness, and natural abundance [23–27]. However, its practical applications are limited due to its poor electrical conductivity and significant volume expansion/contraction during repeated cycling processes. To solve these problems, a porous MnO_2 nanostructure can be an effective way to suppress the fast capacity fading because the porous structure can accommodate a large volume change during charge/discharge cycling. Xia et al. reported a porous nanoflaky MnO_2/CNT nanocomposite

* Corresponding author. Tel.: +82 32 860 7483; fax: +82 32 865 5178.
E-mail address: hjjin@inha.ac.kr (H.-J. Jin).

0378-7753/$ – see front matter © 2012 Elsevier B.V. All rights reserved.
http://dx.doi.org/10.1016/j.jpowsour.2012.11.056

anode, which exhibited a reversible capacity of approximately 600 mA h g^{-1} after 50 cycles [25]. This is a considerable improvement compared to an earlier report that a coaxial MnO_2/CNT array electrode can deliver a reversible capacity of approximately 500 mA h g^{-1} after 15 cycles [26]. More recently, Li et al. reported interconnected porous MnO nanoflakes that exhibited 708.4 mA h g^{-1} at the 200th charge–discharge cycle after cycling with various current densities up to 2460 mA g^{-1} [27]. These results demonstrate the importance of a nanostructured design for inducing high performance of anode materials.

In this study, we designed a unique structure in which mesoporous γ-MnO_2 particles were tightly bound by acid-treated single-walled carbon nanotubes (a-SWCNTs) via simple vacuum filtering methods. The mesoporous γ-MnO_2 particles were evenly dispersed in nanoporous a-SWCNT networks in a tightly bound state, which induced highly flexible free-standing heterogeneous hybrid papers (FHHPs) with no binder or current collector. The FHHPs showed great cycle stability, high reversible capacity, and good rate capability during repetitive charge/discharge tests as LIB anodes.

2. Experimental

2.1. Preparation of a-SWCNTs and mesoporous γ-MnO_2 particles

As-received single-walled carbon nanotubes (SWCNTs, Iljin, Korea) were treated with acid using a procedure reported elsewhere [28]. Briefly, the as-received SWCNTs were treated in an acid mixture (sulphuric acid/nitric acid = 3:1 (*v*/*v*) at 60 °C for 6 h. The mesoporous γ-MnO_2 particles were prepared by template-free self-assembly under ultrasound irradiation [29].

2.2. Preparation of FHHPs based on a-SWCNTs and mesoporous γ-MnO_2 particles

The a-SWCNTs and mesoporous γ-MnO_2 particles were dispersed separately in distilled water by ultrasound treatment. Then, the a-SWCNT dispersion and mesoporous γ-MnO_2 particle dispersion were mixed and stirred for 30 min. The a-SWCNT/mesoporous γ-MnO_2 particle dispersion was then vacuum filtered on an alumina template membrane. After being washed several times by ethanol, the hybrids were dried at room temperature for 24 h.

2.3. Characterization

The morphologies of the a-SWCNTs, mesoporous γ-MnO_2 particles, and FHHPs were observed by field emission transmission electron microscopy (FE-TEM, JEM2100F, JEOL, Japan) and field emission scanning electron microscopy (FE-SEM, S-4300SE, Hitachi, Japan). The porous properties of the mesoporous γ-MnO_2 particles were analysed using nitrogen adsorption and desorption isotherms that were obtained using the surface area and a porosimetry analyser (ASAP 2020, Micromeritics, USA) at −196 °C. The Brunauer–Emmett–Teller (BET) surface areas (S_{BET}) were calculated according to BET theory. X-ray photoelectron spectroscopy (XPS, PHI 5700 ESCA) was performed using monochromated Al Kα radiation (hν = 1486.6 eV). X-ray diffraction (XRD, Rigaku DMAX 2500) of the mesoporous γ-MnO_2 particles was carried out using Cu Kα radiation (wavelength λ = 0.154 nm) operated at 40 kV and 100 mA.

2.4. Electrochemical characterization

The electrochemical performances of the FHHPs based on a-SWCNTs and mesoporous γ-MnO_2 particles were evaluated with a Wonatec automatic battery cycler in a CR2016-type coin cell. The coin cells were assembled in a glove box filled with argon, employing a composite electrode with metallic lithium foil and 1 M $LiPF_6$ (Aldrich 99.99%) dissolved in a solution of ethylene carbonate/dimethyl carbonate/diethyl carbonate (1:2:1 *v*/*v*) as the electrolyte. The cells were galvanostatically cycled between 0.01 and 3.0 V versus Li/Li^+ at various current densities.

3. Results and discussion

Fig. 1 shows the process of preparing the FHHPs based on a-SWCNTs and mesoporous γ-MnO_2 particles. The FHHPs were easily prepared from an aqueous dispersion of a-SWCNTs and mesoporous γ-MnO_2 particles. The a-SWCNTs were homogeneously dispersed in an aqueous solution, which was possible due to presence of surface functional groups induced by the acid treatment. Fig. 2(a) shows the XPS C 1s spectra of the a-SWCNTs. The a-SWCNTs have a –COO peak at 288.4 eV, as well as a main sp^2 C=C peak at 284.2 eV and an sp^3 C–C peak at 285.0 eV. A large number of oxygen groups (15.49 at%) were introduced to the surface of the a-SWCNTs, resulting in nanoporous network structures by simple filtration process (Fig. 2(b)). Mesoporous γ-MnO_2 particles synthesized by a rapid synthetic method had a worm-like morphology and diameters of approximately 800 nm (Fig. 3(a)). The XRD analysis results revealed that the sample had a hexagonal γ-MnO_2 structure with good crystallinity (inset of Fig. 3(b)). The pore structures of the mesoporous γ-MnO_2 particles were examined by measuring the nitrogen adsorption and desorption isotherms at 77 K using BET methods, as presented in Fig. 3(b). The

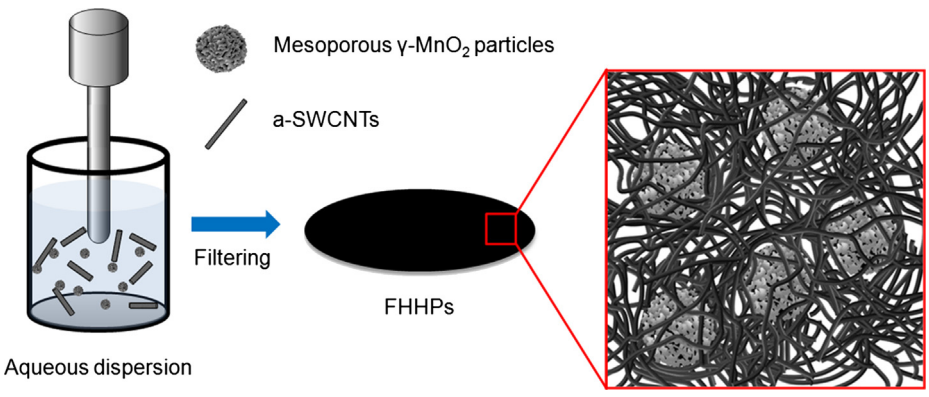

Fig. 1. Schematic processing image of preparing the FHHPs.

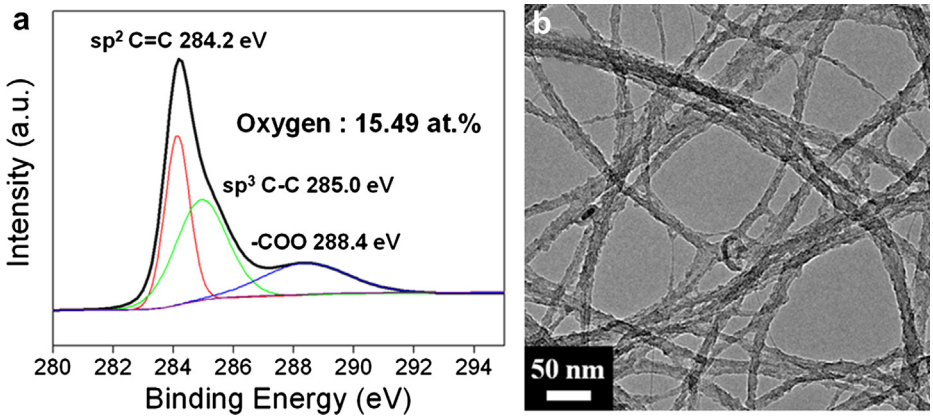

Fig. 2. (a) XPS C 1s spectra and (b) FE-TEM image of a-SWCNTs.

isotherm curve exhibits IUPAC type-IV shapes, indicating a mesoporous structure that can accommodate a large volume change during charge/discharge cycling. In addition, the surface area of the mesoporous γ-MnO_2 particles was 206 m^2 g^{-1}. This high surface area and the porous structure of the active materials can extend the overall reaction area, which is effective for attaining high reversible capacity.

As shown in Fig. 4(a) and (b), the mesoporous γ-MnO_2 particles were practically well distributed in nanoporous a-SWCNT networks in a state thoroughly bound by a-SWCNTs. In addition, the FHHPs had a thickness less than 10 μm, and they spontaneously detached as flexible and free-standing paper from the alumina membrane after they were dried (Fig. 4(c) and (d)). The electrical conductivity of the a-SWCNT paper was 2.8×10^2 S cm^{-1}, which was somewhat lower than that of pristine SWCNT paper (5.2×10^2 S cm^{-1}). This is due to the fact that SWCNT functionalization led to imperfection defects [30]. However, functionalization of SWCNTs by acid treatments can be a good strategy to achieve homogeneous dispersion of SWCNTs and enhanced mechanical properties of buckypaper [31–33]. The electrical conductivity of 30 wt% mesoporous γ-MnO_2 particle-loaded FHHPs (30 wt% FHHPs) and 50 wt% mesoporous γ-MnO_2 particle-loaded FHHPs (50 wt% FHHPs) were 2.5×10^2 S cm^{-1} and 2.4×10^2 S cm^{-1}, respectively. The high electrical conductivities are similar to that of a-SWCNT paper, allowing for a substrate-free and binder-free anode for the FHHPs. Therefore, the FHHPs can have higher energy and simpler fabrication procedures than conventional electrodes.

The electrochemical properties of the a-SWCNT paper, and 30 and 50 wt% FHHPs as LIB anodes with no substrates and no binders were evaluated via constant current charge/discharge cycling in the potential range 0.01–3.0 V at various current densities. During the first charge process (cathodic process) at a current density of 50 mA g^{-1}, the profile of the a-SWCNT paper anode without mesoporous γ-MnO_2 particles shows a large specific capacity in a range below 0.5 V without a distinguishable plateau (Fig. 5(a) and (b)) [34,35]. The reversible capacity is 397 mA h g^{-1} with a coulombic efficiency of 57%. This is equivalent to $Li_{1.1}C_6$, the capacity of which is slightly higher than the ideal value for graphite. In case of FHHP anodes, the profiles exhibit an additional plateau at approximately 0.4 V according to the reaction between MnO_2 and Li, compared to that of the a-SWCNT paper anode (Fig. 5(a) and (b)) [23,25,29,36]. The reversible capacities of the 30 and 50 wt% FHHPs are 658 and 741 mA h g^{-1}, respectively, with coulombic efficiencies of 57% and 58%. After the second cycle, the FHHPs had a smaller irreversible capacity with coulombic efficiencies of above 88%. Fig. 5(c) shows the rate capabilities of the 30 and 50 wt% FHHPs at different current densities ranging from 100 to 1000 mA g^{-1}. To confirm the high reversible capacity, the rate capability was examined again at 100 mA g^{-1}. As the current density was increased, the (discharge) specific capacity of the 30 and 50 wt% FHHPs was maintained at 51% and 48%, respectively, on the basis of the value at 100 mA g^{-1} and quickly stabilized with a minimal change in capacity. In addition, when the current density returned to the initial value of 100 mA g^{-1} after 20 cycles, both anode materials successfully recovered their original capacity. Fig. 5(d) shows that the 30 wt% FHHPs exhibited a stable charge capacity up to 150 cycles except for an initial fluctuation; after 150 cycles, a specific capacity of 754 mA h g^{-1} was maintained. For the 50 wt% FHHPs, there were some capacity fluctuations during the cycling test up to 150 cycles. However, the sample maintained a specific capacity above

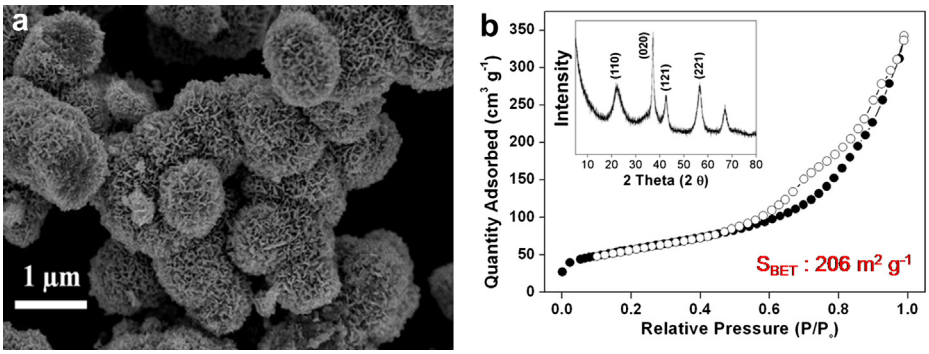

Fig. 3. (a) FE-SEM image and (b) nitrogen adsorption and desorption isotherm of mesoporous γ-MnO_2 particles (inset of (b): XRD data of mesoporous γ-MnO_2 particles).

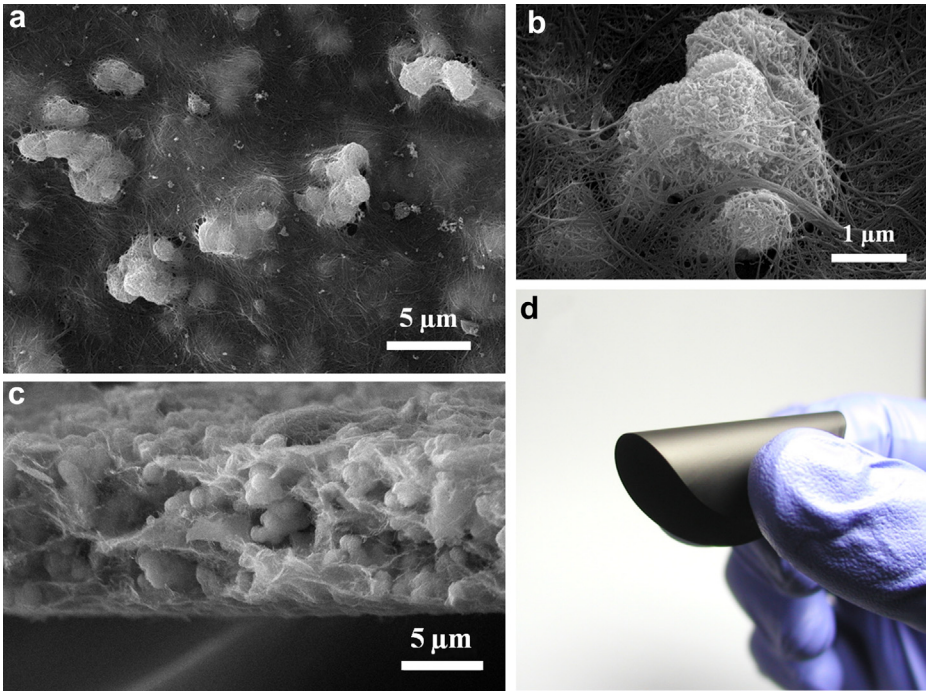

Fig. 4. FE-SEM images of the FHHPs: (a) and (b) upper surface, (c) fracture surface, and (d) optical image.

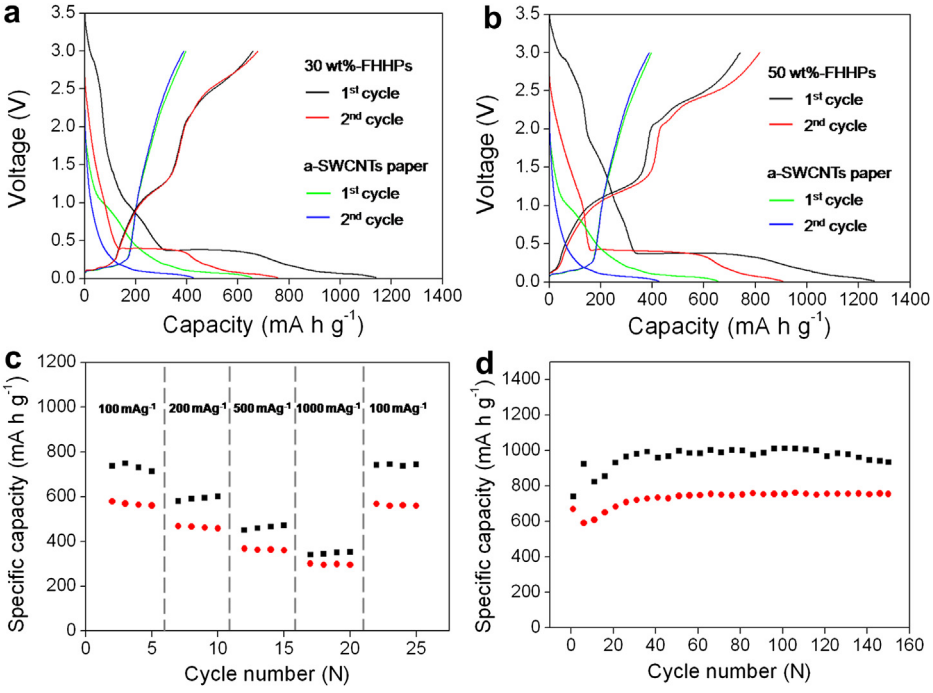

Fig. 5. Galvanostatic charge/discharge profiles of (a) the 30 wt% FHHPs and a-SWCNT paper and (b) the 50 wt% FHHPs and a-SWCNT paper in the potential range from 0.01 to 3.0 V at a current density of 50 mA g^{-1} (discharge). Specific capacity vs. cycle number for the (c) 30 (red circles) and 50 wt% FHHPs (black squares) cycled at different current densities. Cycling performance of the (d) 30 (red circles) and 50 wt% FHHPs (black squares) at 50 mA g^{-1}. (For interpretation of the references to colour in this figure legend, the reader is referred to the web version of this article.)

800 mA h g^{-1} overall, except for the initial 5 cycles. Moreover, after 150 cycles, a specific capacity of 934 mA h g^{-1} could be maintained. These specific capacity values surpass that of mesoporous γ-MnO_2 particles (approximately 400 mA h g^{-1} at 70 mA g^{-1}) [29] because of the nanostructured form with good dispersion of mesoporous γ-MnO_2 particles and a great electroconducting pathway from the a-SWCNT networks. In addition, the nanoporous structure, in which the mesoporous γ-MnO_2 particles were thoroughly bound by a-SWCNTs, induced the good cycling stabilities.

4. Conclusions

FHHPs based on mesoporous γ-MnO_2 particles bound by a-SWCNTs for LIB anodes were successfully prepared by simple

vacuum filtration. The 30 and 50 wt% FHHPs had high electrical conductivities of 2.5×10^2 and 2.4×10^2 S cm^{-1}, respectively, in addition to good rate capabilities and great cycle stabilities. Superior reversible capacities of 754 and 934 mA h g^{-1} (0.01–3.0 V) for the 30 and 50 wt% FHHPs, respectively, remained after 150 cycles. FHHPs have potential for application as a substrate- and binder-free electrode with higher energy and simpler fabrication procedures than conventional electrodes.

Acknowledgements

This work was supported by the National Research Foundation of Korea Grant funded by the Korean Government (MEST) (NRF-2010-C1AAA001-0029018).

References

[1] A.S. Aricò, P. Bruce, B. Scrosati, J.-M. Tarascon, W.V. Schalkwijk, Nat. Mater. 4 (2005) 366–377.
[2] Y.-G. Guo, J.S. Hu, L.-J. Wan, Adv. Mater. 20 (2008) 2878–2887.
[3] H. Gleiter, Acta Mater. 48 (2000) 1–29.
[4] S. Frank, P. Poncharal, Z.L. Wang, W.A. de Heer, Science 280 (1998) 1744–1746.
[5] W. Liang, M. Bockrath, D. Bozovic, J.H. Hafner, M. Tinkham, H. Park, Nature 411 (2001) 665–669.
[6] E.W. Wong, P.E. Sheehan, C.M. Lieber, Science 277 (1997) 1971–1975.
[7] D.A. Walters, L.M. Ericson, M.J. Casavant, J. Liu, D.T. Colbert, K.A. Smith, R.E. Smalley, Appl. Phys. Lett. 74 (1999) 3803–3805.
[8] M. Kociak, A.Y. Kasumov, S. Guéron, B. Reulet, I.I. Khodos, Y.B. Gorbatov, V.T. Volkov, L. Vaccarini, H. Bouchiat, Phys. Rev. Lett. 86 (2001) 2416–2419.
[9] R.H. Baughman, A.A. Zakhidov, W.A. de Heer, Science 297 (2002) 787–792.
[10] L. Hu, H. Wu, Y. Gao, A. Cao, H. Li, J. McDough, X. Xie, M. Zhou, Y. Cui, Adv. Energ. Mater. 1 (2011) 523–527.
[11] I. Lahiri, S.-W. Oh, J.Y. Hwang, S. Cho, Y.-K. Sun, R. Banerjee, W. Choi, ACS Nano 4 (2010) 3440–3446.
[12] W. Wang, P.N. Kumta, ACS Nano 4 (2010) 2233–2241.
[13] S.W. Lee, N. Yabuuchi, B.M. Gallant, S. Chen, B.-S. Kim, P.T. Hammond, Y. Shao-Horn, Nat. Nanotechnol. 5 (2010) 531–537.
[14] R. Liu, J. Duay, S.B. Lee, Chem. Commun. 47 (2011) 1384–1404.
[15] J. Chen, J.Z. Wang, A.I. Minett, Y. Liu, C. Lynam, H. Liu, G.G. Wallace, Energ. Environ. Sci. 2 (2009) 393–396.
[16] S.Y. Chew, S.H. Ng, J. Wang, P. Novak, F. Krumeich, S.L. Chou, J. Chen, H.K. Liu, Carbon 47 (2009) 2976–2983.
[17] S.H. Ng, J. Wang, Z.P. Guo, J. Chen, G.X. Wang, H.K. Liu, Electrochim. Acta 51 (2005) 23–28.
[18] L. Hu, H. Wu, F.L. Mantia, Y. Yang, Y. Cui, ACS Nano 4 (2010) 5843–5848.
[19] P. Poizot, S. Laruelle, S. Grugeon, L. Dupont, J.-M. Tarascon, Nature 407 (2000) 496–499.
[20] N. Ding, X. Feng, S. Liu, J. Xu, X. Fang, I. Lieberwirth, C. Chen, Electrochem. Commun. 11 (2009) 538–541.
[21] M.-Y. Li, Y. Wang, C.-L. Liu, H. Gao, W.-S. Dong, Electrochim. Acta 67 (2012) 187–193.
[22] S.H. Lee, M. Mathews, H. Toghiani, D.O. Wipf, C.U. Pittman Jr., Chem. Mater. 21 (2009) 2306–2314.
[23] M.-S. Wu, P.-C.J. Chiang, Electrochem. Commun. 8 (2006) 383–388.
[24] L. Ji, X. Zhang, Electrochem. Commun. 11 (2009) 795–798.
[25] H. Xia, M. Lai, L. Lu, J. Mater. Chem. 20 (2010) 6896–6902.
[26] A.L.M. Reddy, M.M. Shaijumon, S.R. Gowda, P.M. Ajayan, Nano Lett. 9 (2009) 1002–1006.
[27] X. Li, D. Li, L. Qiao, X. Wang, X. Sun, P. Wang, D. He, J. Mater. Chem. 22 (2012) 9189–9194.
[28] Y.S. Yun, D. Kim, Y. Tak, H.-J. Jin, Synth. Met. 161 (2011) 2460–2465.
[29] J.M. Kim, Y.S. Huh, Y.-K. Han, M.S. Cho, H.J. Kim, Electrochem. Commun. 14 (2012) 32–35.
[30] M.T. Martínez, M.A. Callejas, A.M. Benito, M. Cochet, T. Seeger, A. Ansón, J. Schreiber, C. Gordon, C. Marhic, O. Chauvet, J.L.G. Fierro, W.K. Maser, Carbon 41 (2003) 2247–2256.
[31] G.-W. Lee, S. Kumar, J. Phys. Chem. B 109 (2005) 17128–17133.
[32] X. Zhang, T.V. Sreekumar, T. Liu, S. Kumar, J. Phys. Chem. B 108 (2004) 16435–16440.
[33] T.V. Sreekumar, T. Liu, S. Kumar, Chem. Mater. 15 (2003) 175–178.
[34] E. Yoo, J. Kim, H.-s. Zhou, T. Kudo, I. Honma, Nano Lett. 8 (2008) 2277–2282.
[35] S. Yang, J. Huo, H. Song, X. Chen, Electrochim. Acta 53 (2008) 2238–2244.
[36] M.-S. Wu, P.-C.J. Chiang, J.-T. Lee, J.-C. Lin, J. Phys. Chem. B 109 (2005) 23279–23284.